Numerical Analysis of the Long-Term Performance of Energy Piles in Sand

Kang Fei(✉), Wei Hong, and Jian Qian

Institute of Geotechnical Engineering,
Yangzhou University, Yangzhou 225127, China
kfei@yzu.edu.cn

Abstract. Energy piles are piles equipped with heat exchange pipes through which a heat-carrying fluid circulates and exchanges heat with the ground. This technology couples the structural role of classical pile foundations with the energy supply of heat exchangers. During heating and cooling processes, the temperature of the energy pile and the ground will change seasonally. Due to the thermal displacement incompatibility between the pile and the soil, the load transfer mechanism of energy piles is different to that of conventional piles which are only subjected to mechanical loadings. In order to improve the understanding of the long-term performance of energy piles in sands, a series of coupled thermal-stress finite element analyses were carried out. In the analyses, the bounding surface plasticity model was used to describe the nonlinear behavior of sands under monotonic and cyclic loadings. The thermally induced displacement and axial force in the pile, the thermally induced change in the soil stress, and the ultimate pile resistance after thermal cycles were discussed. The numerical results indicated that the soils around the energy pile were subjected to cyclic mechanical loadings caused by repeated temperature variations. The accumulation of plastic strains resulted in a significant increase in the pile head settlement for the free head pile and a significant decrease in the pile head reaction force for the restrained head pile. During the reloading stage, the thermally induced decrease in the shaft resistance was compensated by the soil dilatancy, the ultimate pile resistance after thermal cycles did not change remarkably.

Keywords: Energy pile · Long-term performance · Thermal cycles
Numerical analysis · Bounding surface plasticity model

1 Introduction

Ground source heat pumps (GSHPs) are one of the most efficient technologies for the geothermal energy utilization. In a conventional GSHP system, the heat exchange is accomplished by circulating a working fluid through the heat transfer pipes installed in bore holes. In order to reduce the installation costs of GSHP systems, the heat transfer pipes may be incorporated into conventional foundation piles. Such piles equipped with fluid carrying pipes are usually called as energy piles or heat exchanger piles (Brandl 2006; Laloui et al. 2006; Adam and Markiewicz 2009). During the heating/cooling operation of a GSHP system, energy piles will be subjected to seasonal temperature

W. Steyn et al. (eds.), *Pavement Materials and Associated Geotechnical Aspects of Civil Infrastructures*, Sustainable Civil Infrastructures,
https://doi.org/10.1007/978-3-319-95759-3_5

variations. The effects of thermal loads on the mechanical behavior of energy piles have attracted the attention of many researchers. Based on the field data measured by Brandl (2006), Laloui et al. (2006), and Bourne-Webb et al. (2009), the maximum thermally induced stresses in the pile were about 100–300 kPa/°C, the exact values mainly depended on the soil and the pile end-restraint conditions. Since the temperature change of energy piles is generally from −15 to +20 °C, the risk of structural damages due to the temperature variation is relatively small (Di Donna and Laloui 2015). The effects of the temperature variation on the pile capacity and the pile settlement have become the focus of research.

According to the field test of an energy pile in dense sand, Wang et al. (2015) reported that the shaft resistance increased at least 14% when the pile temperature increased by about 20 °C. After cooled naturally, the ultimate shaft resistance returned to its initial value, no decrease in the shaft resistance was observed after the heating and recovery cycle. Ng et al. (2015) carried out a series of centrifuge tests on energy piles in medium dense saturated sand. They also found that the pile capacity increased with the pile temperature. This trend is believed to be the result of the increased horizontal stress caused by the radial thermal expansion of the pile (McCartney and Rosenberg 2011). However, Goode et al. (2014) observed that there was no apparent change in the pile capacity based on the centrifuge experiments with dry sand. Olgun et al. (2014) pointed out that the contribution of the radial expansion to the shaft resistance was not as high as expected, the change of the moisture content and the soil mechanical behavior may also have important effects.

It is worth noting that the energy pile will experience seasonally expansion and contraction during the entire service period. As a result, the surrounding soil will be subjected to cyclic loadings, which may have an important impact on the bearing capacity and the settlement of the energy pile, especially for the floating or the semi-floating pile (Suryatriyastuti et al. 2014; Ng et al. 2016). Ng et al. (2014a, b) performed centrifuge tests on floating energy piles in clay. They observed that for the piles in lightly and heavily overconsolidated clay, the cumulative pile settlements after five thermal cycles were 3.8 and 2.1% pile diameter respectively, which were significantly larger than those caused by the static working load. Kalantidou et al. (2012) also studied the effects of temperature cycles on the pile settlement. It was shown that when the mechanical load was high, the irreversible pile settlement after thermal cycles could not be ignored. A similar conclusion has been made by Yavari et al. (2014) using laboratory scale tests. One possible reason for the irreversible settlement is that the thermal deformation of the energy pile may modify the stress state of the surrounding soil and induce the plastic strain.

Saggy and Chakrabotry (2015) investigated the effects of thermal cycles on the pile capacity and the displacement by finite element analyses. In their study, the sand behavior was described by the Mohr-coulomb model. They suggested that the thermal loadings increased the limit shaft resistance for the pile embedded in dense sand, while it has no effect for the pile in loose sand. This phenomenon occurred because the dense sand provided a stronger constraint to the radial expansion of the pile. However, this conclusion may be questioned since the strain softening of the soil and the accumulation of plastic strain during thermal cycles were not modeled reasonably.

At present, the effects of thermal cycles on the changes in the stress state of the soil and the long-term performance of energy piles are not well understood yet. In order to improve the understanding of the long-term performance of energy piles in sand, a series of coupled thermal-stress finite element analyses has been carried out. Based on the results, the mechanical behavior of energy piles during and after thermal cycles was analyzed.

2 Numerical Model Description

2.1 Numerical Analysis Plan

In this study, the long-term performance of single concrete energy piles in both loose and dense dry sand was investigated by ABAQUS software. The modeled piles were 1.0 m in diameter and 20.0 m in length.

For each pile, three sets of analyses have been carried out. In the first set of analyses, the pile was static loaded to failure at a constant temperature. Based on the predicted load-settlement relationship, the ultimate pile resistance was determined.

For the second set of analyses, thermal cycles were applied at the working load level (with a factor of safety of 2.5). Two types of pile head fixities, i.e. a free head pile and a restrained head pile, were considered. The restrained pile considered in this study was an approximation to the single energy pile within a pile group consists of energy and conventional piles. At this situation, the thermally induced displacement at the pile head will be constrained by the raft and can be regarded as zero.

To evaluate the influence of the past thermal cycles on the ultimate pile resistance, the pile was reloaded to failure in the third set of analyses.

2.2 Material Models and Model Parameters

The pile was considered to be thermo-elastic and was modeled as a linear elastic material. The relevant parameters were shown in Table 1.

Table 1. Parameters for the pile

Density ρ kg/m^3	Young's modulus E/GPa	Possion's ratio v	Linear coefficient of thermal expansion $\alpha/10^{-6}$/°C	Thermal conductivity λ/W/(m · °C)	Specific heat c_p/J/(kg · °C)
2500	30	0.18	10	2.0	970

For the dry sands considered in the study, the thermal characteristics were evaluated taking into account the volumetric fractions of the solid soil particles and the pore air. The adopted thermal constants listed in Table 2 were estimated based on the typical values for sand particles

As reported by Yavari et al. (2016), the compressibility and the shear strength of sand was independent of the temperature, so the thermal effects on the mechanical

Table 2. Parameters for the sands

Parameter		Loose Sacramento River sand	Dense Sacramento River sand
Linear coefficient of thermal expansion	$\alpha/10^{-6}/°C$	5.3	6.2
Specific heat	c_p/J/(kg · °C)	946	938
Thermal conductivity	λ/W/(m · °C)	1.34	1.55
Dry density	ρ_d/kg/m^3	1.45	1.67
Elastic swelling modulus	κ	0.0075	0.01
Poisson's ratio	v	0.2	0.2
Critical void ratio at 100 kPa	Γ	0.84	0.97
Slope of critical state line in e–ln p plane	λ	0.076	0.076
Ellipse aspect ratio	ρ	1.65	2.2
Residual friction angle in compression	φ_c/°	36.2	34.6
Residual friction angle in tension	φ_e/°	36.2	34.6
Peak friction angle	φ_p/°	43.8	35.7
Plastic modulus	h_0	2	2

behavior of sands were neglected in the study. To describe the strain softening/hardening, the stress dilatancy and the accumulation of irreversible strains during cyclic loadings, the bounding surface model proposed by Bardet (1986) was used. This model has nine parameters which can be determined from the results of conventional triaxial tests. The values of material constants for loose and dense Sacramento River sand (Bardet 1986) were used in the analyses (Table 2).

The soil-pile interface was modeled by a layer of thin elements, and the constitutive parameters were taken as the same as those for the surrounding sand.

2.3 Initial and Boundary Conditions

The numerical analyses were carried out in axisymmetric conditions. As shown in Fig. 1, the height and the width of the model domain were taken to be 2L and L respectively, where L is the pile length. Both vertical and horizontal displacements were fixed on the bottom of the model domain, and only horizontal displacements were constrained on the lateral sides.

The initial stresses due to gravity were calculated by the bulk unit weights and a coefficient of later earth pressure $K_0 = 0.5$. It should be noted that the pile was considered to be a bored pile, so the installation effects were not considered in the analyses.

The initial temperature of the pile and the ground was 15 °C. To model the thermal operation process of the energy pile, the pile temperature was set to change cyclically.

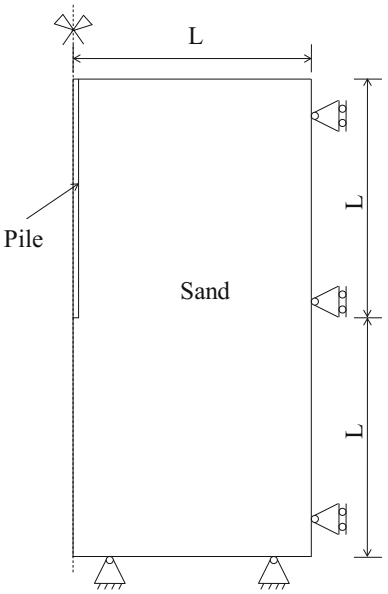

Fig. 1. Sketch of the model

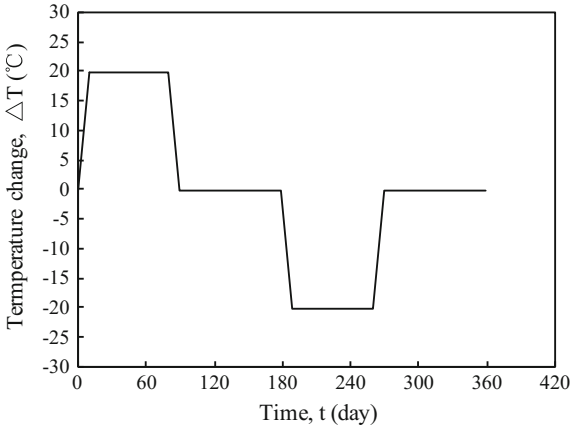

Fig. 2. Temperature variation of pile in one cycle

The temperature variation curve in one cycle is shown in Fig. 2. During the first 90 days (summer mode), the pile temperature was increased by 20 °C in 10 days and then kept constant during the rest time. At the end of this period, the pile temperature was decreased to the initial value and then kept constant for another 90 days. During the following winter mode, the opposite temperature change was applied. In the study, a total of 20 cycles of thermal loading was applied to study the long-term performance.

3 Numerical Results

In this section, the pile response during thermal cycles is analyzed for different pile head fixities. The ultimate pile resistance, the pile displacement, and the pile axial force for all the cases are summarized in Table 3.

3.1 Ultimate Resistances of Piles Without Thermal Cycles

Figure 3 shows the predicted load-settlement relationships for the pile in the loose and dense sand. The results are presented in terms of total resistance Q_t, the shaft resistance Q_s, and the base resistance Q_b. The shaft resistance was mobilized much earlier than the base resistance. The base resistance did not reach a limiting value even at a displacement of 0.1 m. Based on the point where the slope of the load settlement curve significantly decreased, the ultimate pile resistances$Q_u$were 5596 kN (loose sand) and 35,342 kN (dense sand). The corresponding mobilized base resistances were 648kN (Q_b/Q_u = 11.6%) and 6185 kN (Q_b/Q_u = 17.5%) respectively. Since the load was mainly carried by the shaft resistance, both piles were friction piles. By applying a factor of safety of 2.5, the design working load was chosen as 2238 kN and 14,137 kN for the pile in the loose and dense sand respectively.

3.2 Thermally Induced Pile Displacement

3.2.1 Free Head Pile

The displacement distributions of the free head pile after n thermal cycles are shown in Fig. 4. In the figure, downward displacements are taken positive. The letter 1-H and 1-C represent the heating (ΔT = 20 °C) and cooling (ΔT = −20 °C) stage of the first thermal cycle respectively. As expected, the pile expanded during heating and contracted during cooling. For the pile in the loose sand, the pile head heaved by 2.8 mm after the first heating. At the end of the following cooling period, the pile head was 3.2 mm lower than the initial position. Due to the plastic soil strains developed below the pile tip, an irreversible settlement was observed at the pile head when the first thermal cycle finished. The pile head settlement increased gradually to 13.1 mm after 20 cycles, which was about 2.4 times the initial static settlement caused by the mechanical load. The potential influence of the accumulated settlement on the serviceability of the pile and the structure should be considered in the design. For the energy pile in the dense sand, a similar displacement pattern was observed in Fig. 4b. Because the dense sand has higher ability to resist cyclic loading, the increment of the pile settlement was relatively smaller than that for the loose sand. The final settlement was only 1.4 times the initial settlement.

The location of the null point, characterized by zero thermally induced pile displacement, can be identified by comparing the pile displacement distributions at different stages. For the free head pile in the loose sand, the null point of the first heating phase was at a depth of 14.2 m (indicated as NP-H1 in Fig. 4), which was deeper than the midpoint of pile. This phenomenon may be attributed to the increasing soil resistance with the depth. During the subsequent cooling period, the deeper part of the pile-soil interface underwent unloading while the upper part underwent loading. Due to

Table 3. Summary of numerical results

Pile head condition	Soil type	Ultimate pile resistance/kN		Working load/k*N*	Pile head settlement/mm		Maximum change of pile axial force/kN	
		Without thermal cycles	With thermal cycles		Before thermal cycles	After thermal cycles	Compression	Tension
Free	Loose sand	5596	4850	2238	5.5	13.1	591	290
	Dense sand	35,342	34,400	14,137	29.8	42.6	317	384
Restrained	Loose sand	5596	4700	2238	5.5	5.5	1170	−6239
	Dense sand	35,342	34,280	14,137	29.8	29.8	1299	−9064

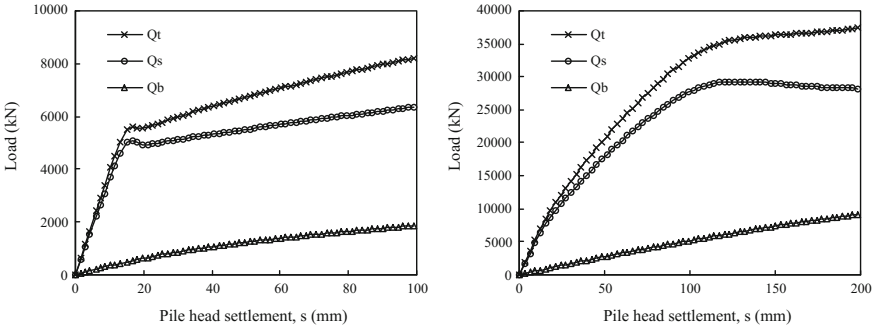

Fig. 3. Load-settlement relationships

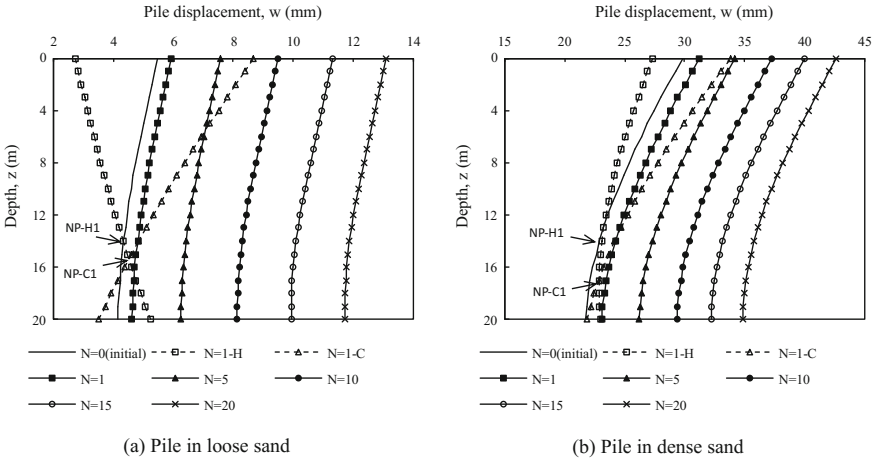

Fig. 4. Displacement distribution of free head pile

the difference between the loading and unloading stiffness, the pile's contraction mobilized greater resistance over the lower section, and thus the null point of the cooling (NP-C1) was deeper that of the heating phase, at around 15.8 m depth. During the subsequent cycles, the locations of the null points did not change significantly. For the pile in the dense sand, the location of the null point varied from 13.2 m (heating) to 16.8 m (cooling).

3.2.2 Restrained Head Pile

For the restrained pile, the pile head was fixed at the beginning of the thermal cycles, so the whole part of the pile displaced in the same direction when heated or cooled (Fig. 5). In other words, the null point of the restrained pile was always at the pile head.

Another important finding is that the displacement at the pile tip increased with the number of thermal cycles, which indicated that the restrained head pile has a tendency

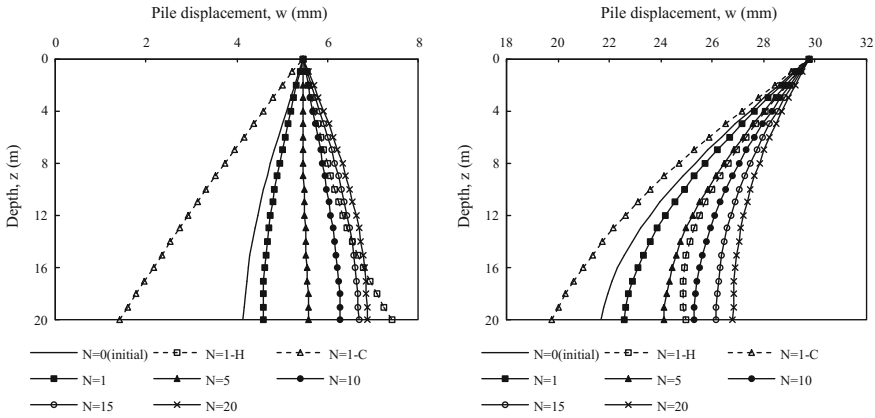

Fig. 5. Displacement distribution of restrained head pile

to elongate during thermal cycles. The main reason for this phenomenon is that the soil experienced significant plastic strains induced by the cyclic loading, so the soil settled more than the pile. Therefore, a downdrag load (or negative shear stress) was induced along the interface of the pile and the soil. Because the loose sand was easier to deform, the thermal cycles resulted in a more significant increase in the axial elongation of the pile. At the end of the thermal operation, the pile in the loose sand was in tension for the entire length.

3.3 Thermally Induced Axial Force in Pile

3.3.1 Free Head Pile

The profiles of the axial force P at different times were shown in Figs. 6 and 7. It is obvious that the effects of thermal cycles on the axial forces depended on the restraint condition and the ground type. For the free head pile in the loose sand, the axial force distribution during the first thermal cycle agreed well with that observed by Bourne-Webb et al. (2009) for the pile which was unrestrained at the pile top and partially restrained at the pile toe. The maximum changes occurred slightly below the mid-depth point. The increment in the axial force was about 280 kN (20% of the initial value at the same depth) for eating and −290 kN (26%) for cooling. After one thermal cycle, a small increase and decrease of the axial force was observed for the upper and the lower part of the pile, respectively. The change of the axial force was observed to increase with the number of thermal cycles. Due to the accumulation of the residual stress, the long-term distribution of the axial load was quite different to the initial shape. After the end of the thermal operation, the axial load first increased and then decreased with the depth. The arising of this phenomenon can be related to the relative displacement between the pile and the soil. Along the lower part of the pile, the pile section moved downward due to the deformation of the soil under the pile base, so the skin force was increased. While at the upper part of the soil, the negative skin force was

generated due to the settlement of the soil caused by stress reversals. For the free head pile in the dense sand (Fig. 6b), the variation of the axial force was relative small due to the large static load and the high stiffness of the dense sand.

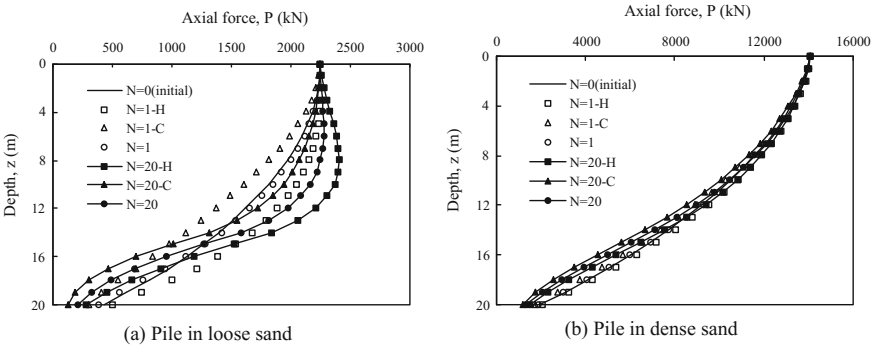

Fig. 6. Axial force distribution of free head pile

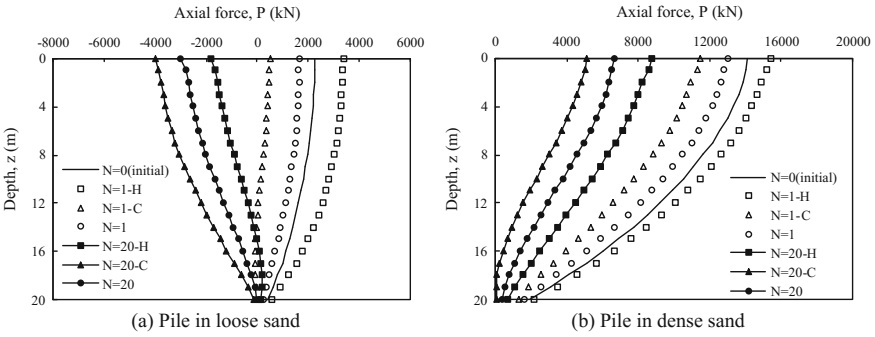

Fig. 7. Axial force distribution of restrained head pile

3.3.2 Restrained Head Pile

If the pile head was fixed during thermal cycles, the compressive axial forces were found to decrease with cycles for both piles in the loose and dense sand. Corresponding to the displacement results in Fig. 5, the reduction in the axial force was more apparent for the pile in the loose sand. In this case, the maximum tensile force developed at the pile head was 4010 kN (5105 kPa). The risk of tensile failure should be considered in the design. It is also worth mention that in a pile group, the reduction of the pile head reaction will generate an additional load on the neighboring pile. The redistribution of stresses should also be taken into account.

3.4 Thermally Induced Change in Soil Stress

3.4.1 Free Head Pile

The stress paths of the soil elements adjacent to the pile shaft at 8, 15, and 18 m depths during and after thermal cycles are shown in Fig. 8. The results of the pile without thermal cycles are also given in the figure for reference. The corresponding shear stress at the pile-soil interface is plotted against the shear strain in Fig. 9. During the axial loading of the pile in the loose sand, the soil elements at depth depths (z = 15 and 18 m) were observed to be contractive and the mean stress decreased with the increase of the deviatoric stress. After the phase transformation state was passed, the soil dilated slightly and the stress path was inverted from left to right to reach the critical state. At shallower depth (z = 8 m), the soil was easy to dilate since the confining stresses were relatively small. Because the tendency to dilate was constrained by the pile shaft, the horizontal stress and the mobilized shear stress increased gradually. For the case of dense sand, the effect of dilation was more obvious. The shear stresses developed continuously while the stress states moved along the failure surface until constant soil volumes were reached at large shear strains.

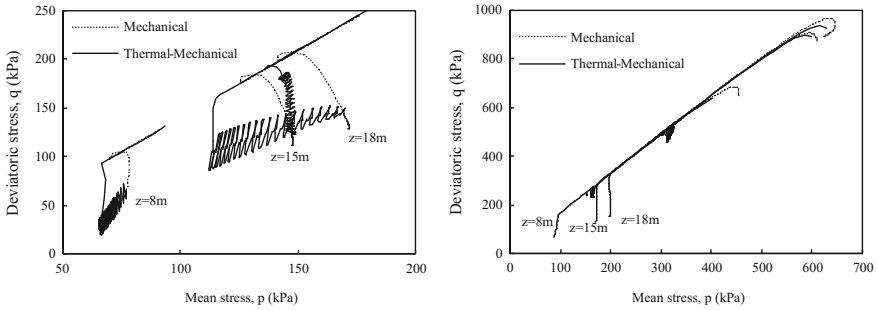

(a) Pile in loose sand (b) Pile in dense sand

Fig. 8. Stress path at pile-soil interface of free head pile

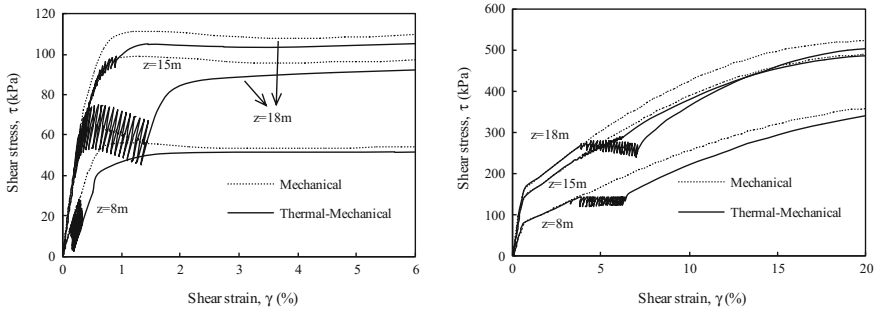

(a) Pile in loose sand (b) Pile in dense sand

Fig. 9. Development of shear stress at pile-soil interface of free head pile

During thermal cycles, different patterns of stress responses were observed for the soils at different depths. This occurrence can be associated to the specific displacement mode developed at these locations. Below the null point, the thermally induced expansion pushed down the pile and led to an increase in the shear stress. For the upper part of the pile, the upward expansive deformation decreased the relative pile-soil displacement and the shear stress. During the process of cooling, the opposite variation of the shear stress would occur. As expected, the shear stresses of the soils at z = 8 and z = 18 m changed cyclically. However, because the null point of cooling was deeper than the null point of heating, the shear deformation of the soil between these two points was always increased during the heating/cooling cycles. Hence, the soil at z = 15 m was sheared monotonically and the response was similar to that of the pile subjected to mechanical loading case.

Because the amplitude of the pile expansion/contraction was mainly controlled by the temperature change and could be regarded as constant during thermal cycles. For the soils at z = 8 and 18 m, the soils were cyclic loaded in the stain controlled condition. Due to the accumulation of plastic strains in each cycle, the mean stresses and the shear stresses at the pile-soil interface decreased with the number of thermal cycles. The reduction of stresses was more apparent for the pile in the loose sand. This tendency of progressive reduction in the stress was consistent with that observed during the dynamic installation of piles. As a result, the stress paths moved progressively to the bottom left. For the soil at z = 15 m, because the soil was nearly sheared in a monotonic way during thermal cycles, the trajectory of the stress path was close to that under the static load. The increase of the shear stress near this point compensated for the friction fatigue at other depths, so the force equilibrium of the pile was maintained.

3.4.2 Restrained Head Pile

In this case, because the null point of the heating and cooling was fixed at the pile head, the shear stresses along the entire length of the pile increased simultaneously during heating and decreased simultaneously during cooling. Because the response at z = 15 m was similar to that at z = 18 m, only the results of the soil at z = 8 and 18 m are given in Figs. 10 and 11. As shown, the reductions of the mean stresses and the shear stresses were also evident. Because the thermal induced displacement of the pile increased with the distance to the null point, the variations of soil stresses were more apparent at deeper locations. For example, the reduction of the mean stress at z = 8 and 18 m were 17.3% and 36.3% for the pile in the loose sand, and were 7.2% and 43.0% in the case of dense sand. Due to the same reason, the decrease in the shear stress at z = 18 m was larger than that in the free head pile case. For the pile in loose sand, a negative shear stress was observed before the reloading started.

3.5 Ultimate Pile Resistance After Thermal Cycles

3.5.1 Free Head Pile

As shown in Fig. 9, for the free head pile in loose sand, the ultimate shear resistance mobilized at z = 8 m was 51.3 kPa, which was only 2.7 kPa less than that in the case of pile without thermal cycles. It implies that the stress reduction at this location after thermal cycles was almost fully compensated by the soil dilatancy during the reloading

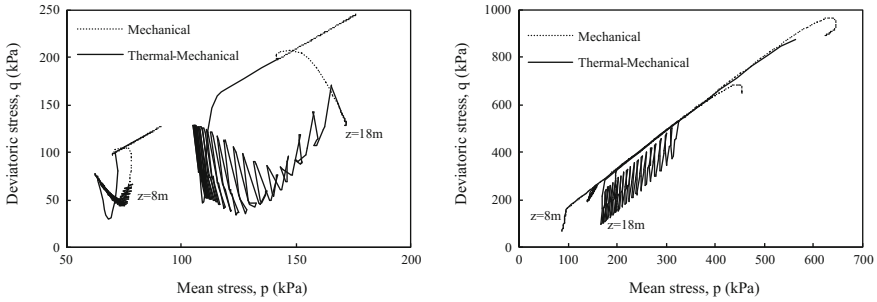

(a) Pile in loose sand (b) Pile in dense sand

Fig. 10. Stress path at pile-soil interface of restrained head pile

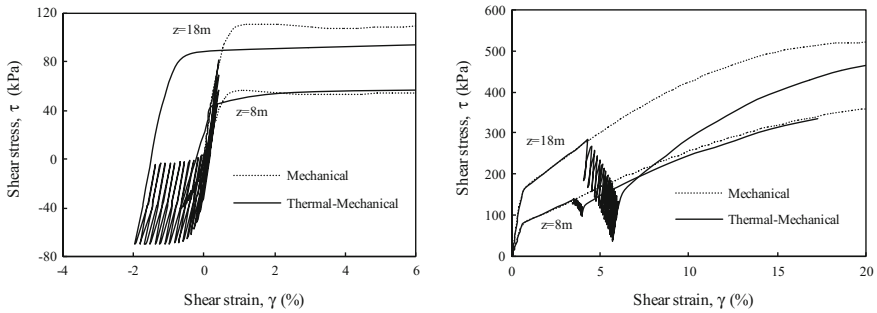

(a) Pile in loose sand (b) Pile in dense sand

Fig. 11. Development of shear stress at pile-soil interface of free head pile

stage. A different tendency was observed for the soil at z = 18 m. With the soil parameters applied and the specific stress condition, the soil was contractive in the subsequent reloading. The change of the soil state after thermal cycles decreased the ultimate shear resistance form 115.3 kPa to 88.2 kPa. For the soil at z = 15 m, the ultimate shear resistance was increased from 97.2 kPa to 106.9 kPa due to the increased horizontal stress after thermal cycles. Similar findings can also be found for the pile in dense sand.

To investigate the effect of thermal cycles on the long-term capacity, the load settlement curves with and without the thermal cycles are compared in Fig. 12. Since the load was mainly undertaken by the shaft resistance, the densification of the soil beneath the pile toe contributed little to the ultimate pile resistance and the load-settlement relationship. As mentioned before, the stress reduction maybe fully or partially compensated by the soil dilatancy, hence the magnitude of the total resistance did not change much. After 20 thermal cycles, the decreases in the total ultimate resistance were 13 and 3% for the free head pile in the loose and dense sand. It should

be noted that due to the degradation effect at the pile-soil interface and the change in the soil state, the pile displacement required to mobilize ultimate resistance increased after thermal cycles. The overall stiffness of the pile-soil system decreased slightly after thermal cycles. Also taking into account the accumulated settlement during the thermal operation, the long-term performance of the energy pile seems to be mainly controlled by the settlement rather than the capacity.

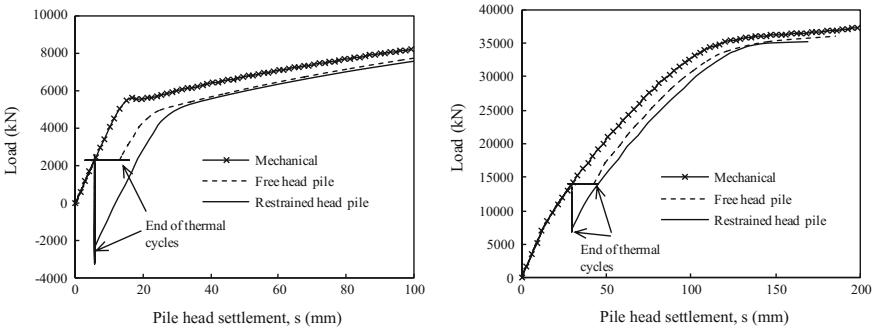

Fig. 12. Comparison of load settlement curves of piles with and without thermal cycles

3.5.2 Restrained Head Pile

The load settlement curves of restrained head piles in the loose and dense sand are also plotted in Fig. 12. Though the negative shear stress may be induced by the application of thermal cycles, the pile will move down relative to the soil in the subsequent reloading stage, and the negative shear stress will be eliminated. Similar to that observed for free head piles, the reductions of the horizontal stress and the mobilized shear stress recovered to a large extent in the subsequent reloading. The total resistances were reduced by 16% and 3% for the piles in loose and dense sand.

4 Conclusion

To improve the understanding of the effects of thermal cycles on the long-term performance of the single energy pile, coupled thermal-stress analyses were carried out. Based on the results, the following conclusions may be drawn:

(1) Due to the irreversible soil strains caused by cyclic loadings, the pile head settlement for the free head pile increased with the number of thermal cycles. After 20 cycles, the pile head settlement was 2.4 and 1.4 times the initial static settlement for the pile in the loose and dense sand, respectively. For the restrained head pile, a significant decrease in the pile head reaction was observed. For this case, the risk of tensile failure should be considered.

(2) The free head pile tended to have different development patterns of the shear stresses at different depths. For the soils located between the null point of heating

and the null point of cooling, the shear stresses developed monotonically despite the cyclic loading condition, while the reductions of the horizontal stress and the shear stress were observed for the other parts of the pile. In the case of the restrained head pile, the stress reduction was observed along the entire length of the pile.

(3) The reduction of the shaft resistance was recovered remarkably due to the soil dilatancy in the subsequent reloading. Comparing with piles subjected to mechanical loads, the ultimate pile resistance was reduced in the range of 13% to 16% for piles in the loose sand, and was reduced by 3% for those in the dense sand. Therefore, for the long-term design of energy piles in sand, the main problem is the settlement rather than the bearing capacity.

Acknowledgements. The authors acknowledge the support from the National Natural Science Foundation of China (No. 51778557) and the Qing Lan Project (No. 20160512) by the Jiangsu Province Government.

References

Adam D., Markiewicz R.: Energy from earth-coupled structures, foundations, tunnels and sewers. Géotechnique **59**(3), 229–236 (2009). https://doi.org/10.1680/geot.2009.59.3.229

Bardet, J.P.: Bounding surface plasticity model for sands. J. Eng. Mech. **112**(11), 1198–1217 (1986). https://doi.org/10.1061/(ASCE)0733-9399(1986)112:11(1198)

Bourne-Webb, P.J., Amatya, B., Soga, K., Amis, T., Davidson, C., Payne, P.: Energy pile test at Lambeth College, London: geotechnical and thermodynamic aspects of pile response to heat cycles. Géotechnique **59**(3), 237–248 (2009). https://doi.org/10.1680/geot.2009.59.3.237

Brandl, H.: Energy foundations and other thermo-active ground structures. Geotechnique **56**(2), 81–122 (2006). https://doi.org/10.1680/geot.2006.56.2.81

Di Donna, A., Laloui, L.: Numerical analysis of the geotechnical behaviour of energy piles. Int. J. Numer. Anal. Meth. Geomech. **39**(8), 861–888 (2015). https://doi.org/10.1002/nag.2341

Goode III J.C., Zhang M., McCartney J.S.: Centrifuge modelling of energy foundations in sand. In: ICPMG2014—Physical Modelling in Geotechnics: Proceedings of the 8th International Conference on Physical Modelling in Geotechnics 2014 (ICPMG2014), Perth, Australia, 14–17 January 2014, pp. 729–735 (2014). https://doi.org/10.1201/b16200-100

Kalantidou, A., Tang, A.M., Pereira, J.M., Hassen, G.: Preliminary study on the mechanical behaviour of heat exchanger pile in physical model. Géotechnique **62**(11), 1047–1051 (2012). https://doi.org/10.1680/geot.11.T.013

Laloui, L., Nuth, M., Vulliet, L.: Experimental and numerical investigations of the behaviour of a heat exchanger pile. Int. J. Numer. Anal. Meth. Geomech. **30**(8), 763–781 (2006). https://doi.org/10.1002/nag.499

McCartney J.S., Rosenberg J.E. (2011) Impact of heat exchange on side shear in thermo-active foundations. In: Geo-Frontiers 2011: advances in geotechnical engineering pp. 488–498. https://doi.org/10.1061/41165(397)51

Ng, C.W.W., Shi, C., Gunawan, A., Laloui, L.: Centrifuge modelling of energy piles subjected to heating and cooling cycles in clay. Geotechnique Lett. **4**(4), 310–315 (2014a). https://doi.org/10.1680/geolett.14.00063

Ng, C.W.W., Shi, C., Gunawan, A., Laloui, L., Liu, H.L.: Centrifuge modelling of heating effects on energy pile performance in saturated sand. Can. Geotech. J. **52**(8), 1045–1057 (2014b). https://doi.org/10.1139/cgj-2014-0301

Olgun, C.G., Ozudogru, T.Y., Arson, C.F.: Thermo-mechanical radial expansion of heat exchanger piles and possible effects on contact pressures at pile-soil interface. Geotechnique Lett. **4**, 170–178 (2014). https://doi.org/10.1680/geolett.14.00018

Wang, B., Bouazza, A., Rao, M.S., Haberfield, C., Barry-Macaulay, D., Baycan, S.: Posttemperature effects on shaft capacity of a full-scale geothermal energy pile. J. Geotechnical, Geoenvironmental Eng. **141**(4), 04014125 (2015). https://doi.org/10.1061/(ASCE)GT.1943-5606.0001266

Yavari, N., Tang, A.M., Pereira, J.M., Hassen, G.: Experimental study on the mechanical behaviour of a heat exchanger pile using physical modelling. Acta Geotech. **9**(3), 385–398 (2014). https://doi.org/10.1007/s11440-014-0310-7